Science Advances
AAAS

Supplementary Materials for

TisB protein is the single molecular determinant underlying multiple downstream effects of ofloxacin in *Escherichia coli*

Julien Cayron *et al.*

Corresponding author: Laurence Van Melderen, laurence.van.melderen@ulb.be

Sci. Adv. **10**, eadk1577 (2024)
DOI: 10.1126/sciadv.adk1577

The PDF file includes:

Other Supplementary Material for this manuscript includes the following:

Supplementary figures

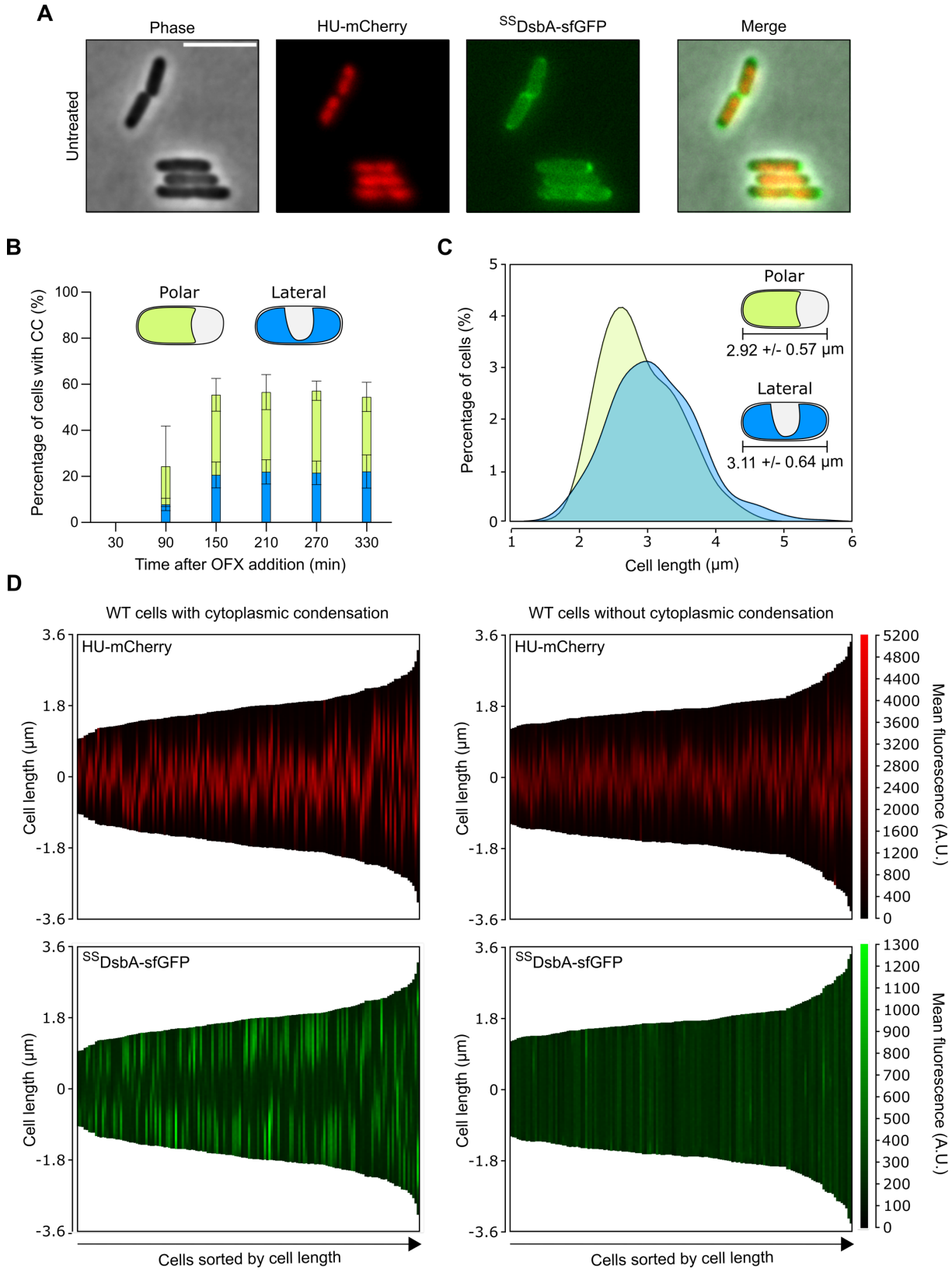

Figure S1: Polar and lateral cytoplasmic condensation are independent of cell length and lead to a displacement of the nucleoid

For all experiments, cells were grown in MOPS 0.4% glucose at 37°C to an OD_{600nm} ~ 0.3 and treated as described. Results are representative of 3 biological replicates. The data points are mean ± SD. (A) Snapshots of untreated wild-type (WT) encoding a *hupA-mCherry* fusion and an IPTG-inducible periplasmic marker ^{SS}*dsbA-sfgfp*. The strain was grown in presence of 250 µM IPTG and spotted onto agarose pads containing 250 µM IPTG. Phase contrast, mCherry (fire) and GFP (green) channels are shown as well as the merge of the fluorescence channels. Scale bar = 5 µm. (B-C) WT cells were spotted onto agarose pads containing 5 µg/mL OFX. Time-lapse image acquisition started 5 min after spotting with additional image acquisition every 5 min. (B) Percentage of WT cells in which polar (green) or lateral (blue) cytoplasmic condensation is detected after OFX. (C) Cell length distribution of WT cells undergoing polar (green) or lateral (blue) cytoplasmic condensation after 240 min in the presence of 5 µg/mL OFX. Between 372 and 669 were analyzed for each condition. (D) Demographs of HU-mCherry (upper panels) and ^{SS}DsbA-sfGFP (lower panels) localization in WT with (left panels) or without (right panels) cytoplasmic condensation 120 min after addition of OFX. WT encoding a *hupA-mCherry* fusion and an IPTG-inducible periplasmic marker ^{SS}*dsbA-sfgfp* was grown in presence of 250 µM IPTG and treated with 5 µg/mL OFX. Cells were then spotted onto agarose pads containing 250 µM IPTG 120 min after addition of OFX. A total of 100 cells analyzed. Cells are sorted by cell length. A.U. for arbitrary units.

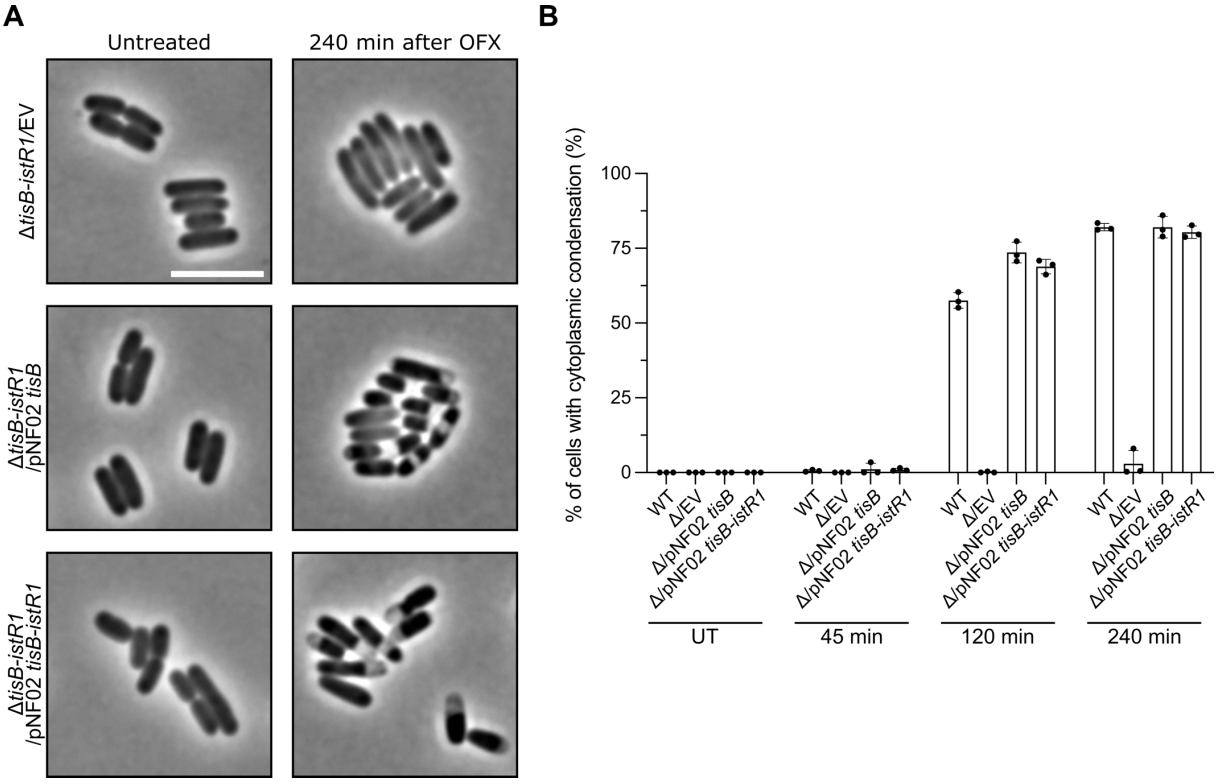

Figure S2: Complementation of ΔtisB-istR1 mutant with a plasmid containing tisB restores the cytoplasmic condensation phenotype

For all experiments, Δ*tisB-istR1* strains carrying either the empty vector plasmid (EV), a plasmid containing *tisB* under native transcriptional regulation (pNF02 *tisB*) or a plasmid containing the entire *tisB-istR1* locus under native transcriptional regulation (pNF02 *tisB-istR1*) were grown in MOPS 0.4% glucose at 37°C to an OD_{600nm} ~ 0.3 and treated with 5 µg/mL OFX. At indicated times, cells were spotted onto agarose pads and imaged. Results are representative of 3 biological replicates. (A) Representative images before and 240 min after OFX addition. Scale bar = 5 µm. (B) Percentage of Δ*tisB-istR1/EV* (Δ*/EV*), Δ*tisB-istR1/*pNF02 *tisB* (Δ/pNF02 *tisB*), and Δ*tisB-istR1/*pNF02 *tisB-istR1* (Δ/pNF02 *tisB-istR1*) cells in which cytoplasmic condensation (CC) is detected after OFX addition. Results for WT cells are from figure 2B. Between 162 and 1,137 cells were analyzed for each sample. The data points are mean ± SD.

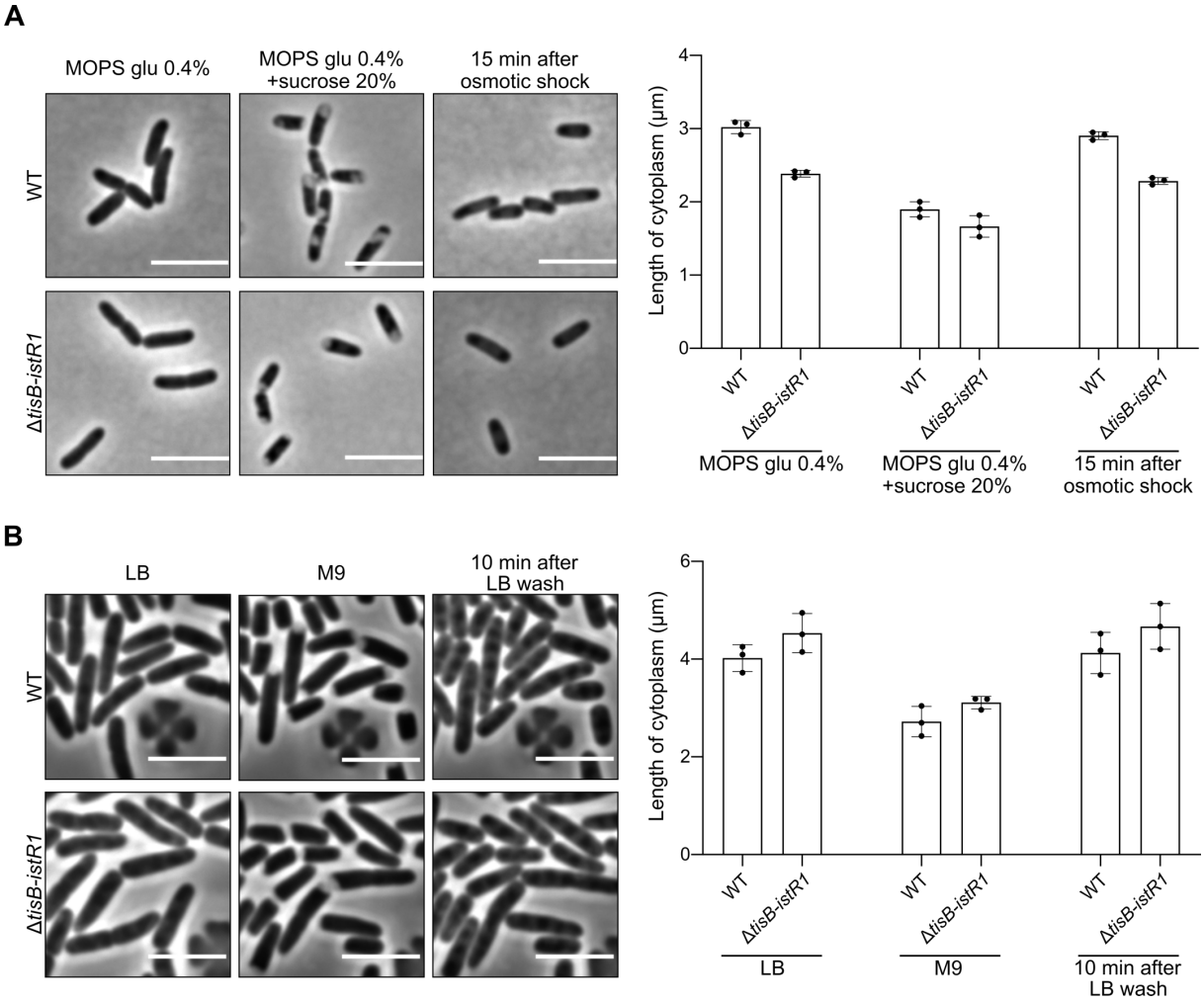

Figure S3: Osmotic shock and nutriment downshift induce tisB-independent cytoplasmic condensation

(A) Length of cytoplasm before, during and 15 min after sucrose-induced osmotic shock in WT and Δ*tisB-istR1* derivative. Left panel: Representative images of WT and Δ*tisB-istR1* cells. Right panel: Quantification of cytoplasm length. WT and Δ*tisB-istR1* derivative were grown in MOPS 0.4% glucose at 37°C to an OD_{600nm} ~ 0.3. Cells were spotted onto agarose pads with or without 20% sucrose and imaged immediately or 15 min after spotting. Results are representative of 3 biological replicates. Between 412 and 939 cells analyzed for each condition. The data points are mean ± SD. Scale bar = 5 µm. (B) Length of cytoplasm before, during (2 h after M9 perfusion) and 10 min after perfusion with LB in WT and Δ*tisB-istR1* cells. Left panel:

Representative images of WT and Δ*tisB-istR1* cells. Right panel: Quantification of cytoplasm length. WT and Δ*tisB-istR1* cells were grown in the microfluidic device in LB 37°C for 60 min. Cells were then perfused with M9 for 2 h followed by 1 h of perfusion with LB. Image acquisition was performed every 10 min. Results are representative of 3 biological replicates. Between 65 to 412 cells were analyzed for each sample. The data points are mean ± SD. Scale bar = 5 µm.

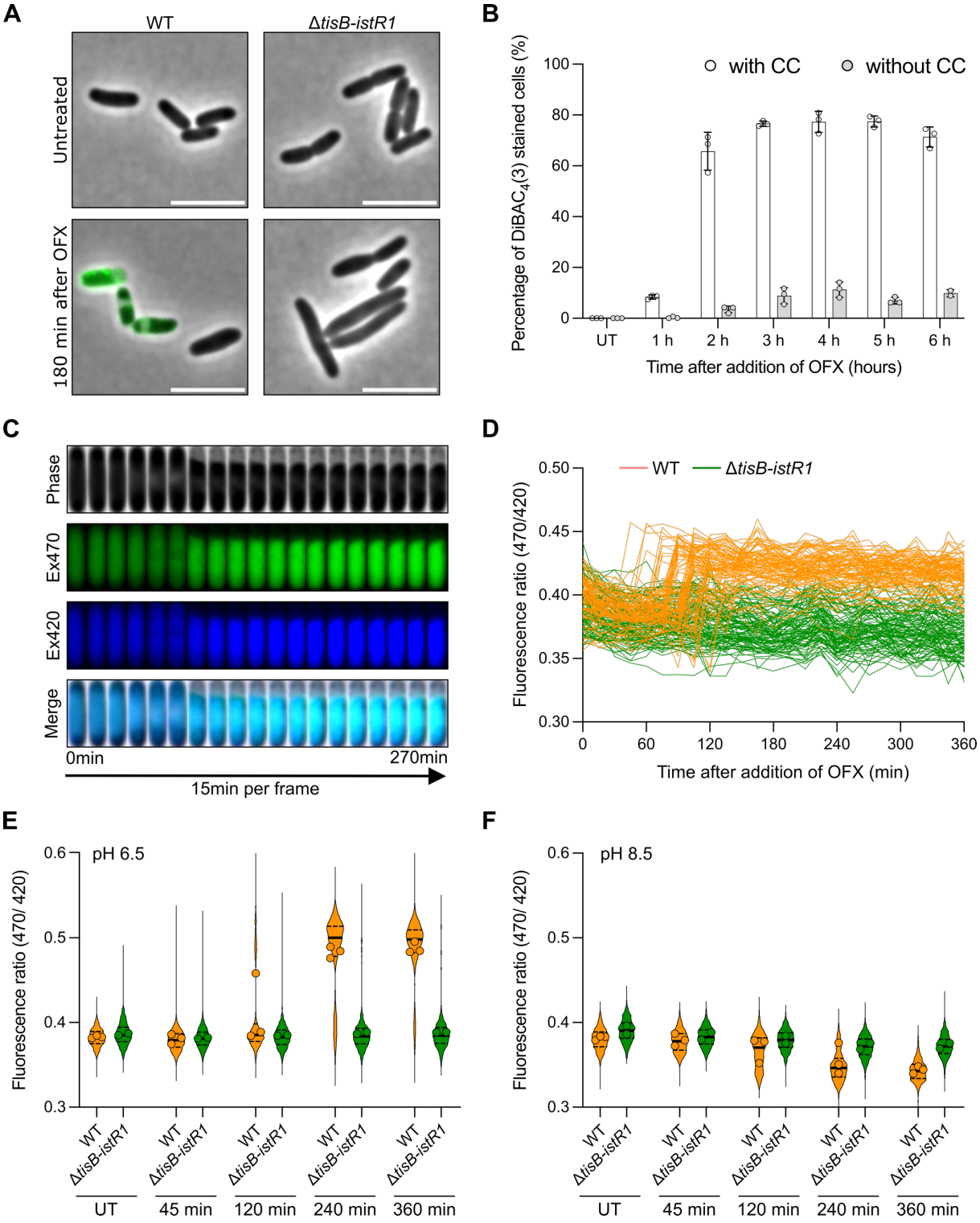

Figure S4: Membrane depolarization and cytoplasmic pH variations are associated with cytoplasmic condensation

(A-B) WT and Δ*tisB-istR1* cells were grown in MOPS 0.4% glucose at 37°C to an OD_{600nm} ~ 0.3 and treated with 5 µg/mL OFX. At indicated times, cells were stained with $DiBAC_4(3)$, spotted

on agarose pads and imaged. Results are representative of 3 biological replicates. (A) Representative images of $DiBAC_4(3)$-staining of WT and Δ*tisB-istR1* cells before and 180 min after OFX treatment. $DiBAC_4(3)$ fluorescence is highlighted in green. Scale bar = 5 µm. (B) Percentage of $DiBAC_4(3)$-stained WT cells with or without cytoplasmic condensation (CC) after OFX addition. Between 376 and 1,555 cells were analyzed for each sample. The data points are mean ± SD. (C-D) WT and its Δ*tisB-istR1* cells containing the pHluorin2 reporter were grown in MOPS 0.4% glucose at 37°C to an OD_{600nm} ~ 0.3, introduced into microfluidic device and perfused with culture medium for 60 min. Cells were then perfused with culture medium containing 5 µg/mL OFX for 360 min. Image acquisition was performed every 15 min. Results are representative of 3 biological replicates. (C) Representative kymograph of WT cells containing pHluorin2 during OFX treatment. Phase contrast, fluorescence at 470 nm (green), fluorescence at 420 nm (dark blue) channels are shown as well as the merge of the fluorescence channels. (D) Single-cell intracellular pH variations during OFX treatment. For each acquisition, the fluorescence ratio (470/420 nm) of individual cells was calculated. A total of 126 and 102 cells were analyzed for WT and the Δ*tisB-istR1* strains, respectively. (E) Intracellular pH variations during OFX treatment in MOPS 0.4% glucose adjusted to pH 6.5. WT and its Δ*tisB-istR1* cells containing the pHluorin2 reporter were grown in MOPS 0.4% glucose adjusted to pH 6.5 at 37°C to an OD_{600nm} ~ 0.3, introduced into microfluidic device and perfused with pH-adjusted culture medium for 60 min. Cells were then perfused with pH-adjusted culture medium containing 5 µg/mL OFX for 360 min. Image acquisition was performed every 15 min. At indicated times, the fluorescence ratio (470/420 nm) of individual cells was calculated. Results are representative of 3 biological replicates. The data points are mean of individual replicate (symbol), median (full line) ± quartiles (dashed line). (F) Same as

(E) but with MOPS glucose 0.4% adjusted to pH 8.5. Between 178 and 1,011 cells were analyzed for each sample.

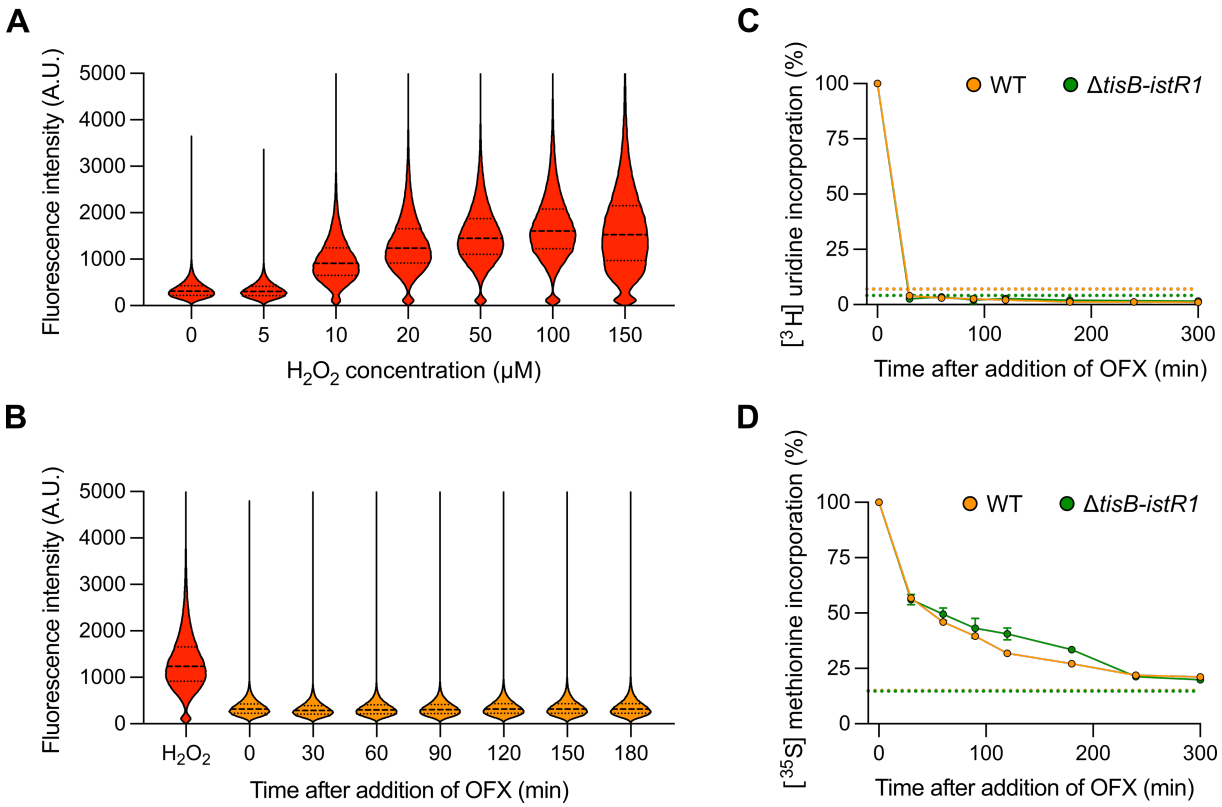

Figure S5: A pkatG::gfp transcriptional reporter is not induced by OFX due to inhibition of transcription

For all experiments, cells were grown in MOPS 0.4% glucose at 37°C to an OD_{600nm} ~ 0.3 and treated as described. Results are representative of 3 biological replicates. (A) Validation of the transcriptional p*katG* reporter. WT cells containing the plasmid-encoded p*katG-gfp*$_{mut2}$ reporter exposed for 30 min to indicated concentrations of H_2O_2 followed by measurement of GFP fluorescence by flow cytometry. A total of 50,000 cells were analyzed per replicate. The data points are median (full line) ± quartiles (dashed line). (B) Induction of transcriptional p*katG-gfp*$_{mut2}$ reporter during OFX treatment. WT cells containing plasmid encoded p*katG-gfp*$_{mut2}$ reporter were treated with 5 µg/mL OFX. At indicated time points, GFP fluorescence

was measured by flow cytometry. H_2O_2 (20 μM) was used as positive control. A total of 50,000 cells were analyzed per replicate. The data points are median (full line) ± quartiles (dashed line). (C) Incorporation of radioactive [^{3}H]-uridine during OFX treatment. WT and Δ*tisB-istR1* strains were treated with 5 μg/mL OFX. At indicated times, culture samples were incubated with radioactive [^{3}H]-uridine for 5 min followed by trichloroacetic acid wash. Dashed line represents mean [^{3}H]-uridine incorporation after 30 min rifampicin. The data points are mean ± SD. (D) Same as (C) but with radioactive [^{35}S]-methionine. Dashed line represents mean [^{35}S]-methionine incorporation after 30 min chloramphenicol.

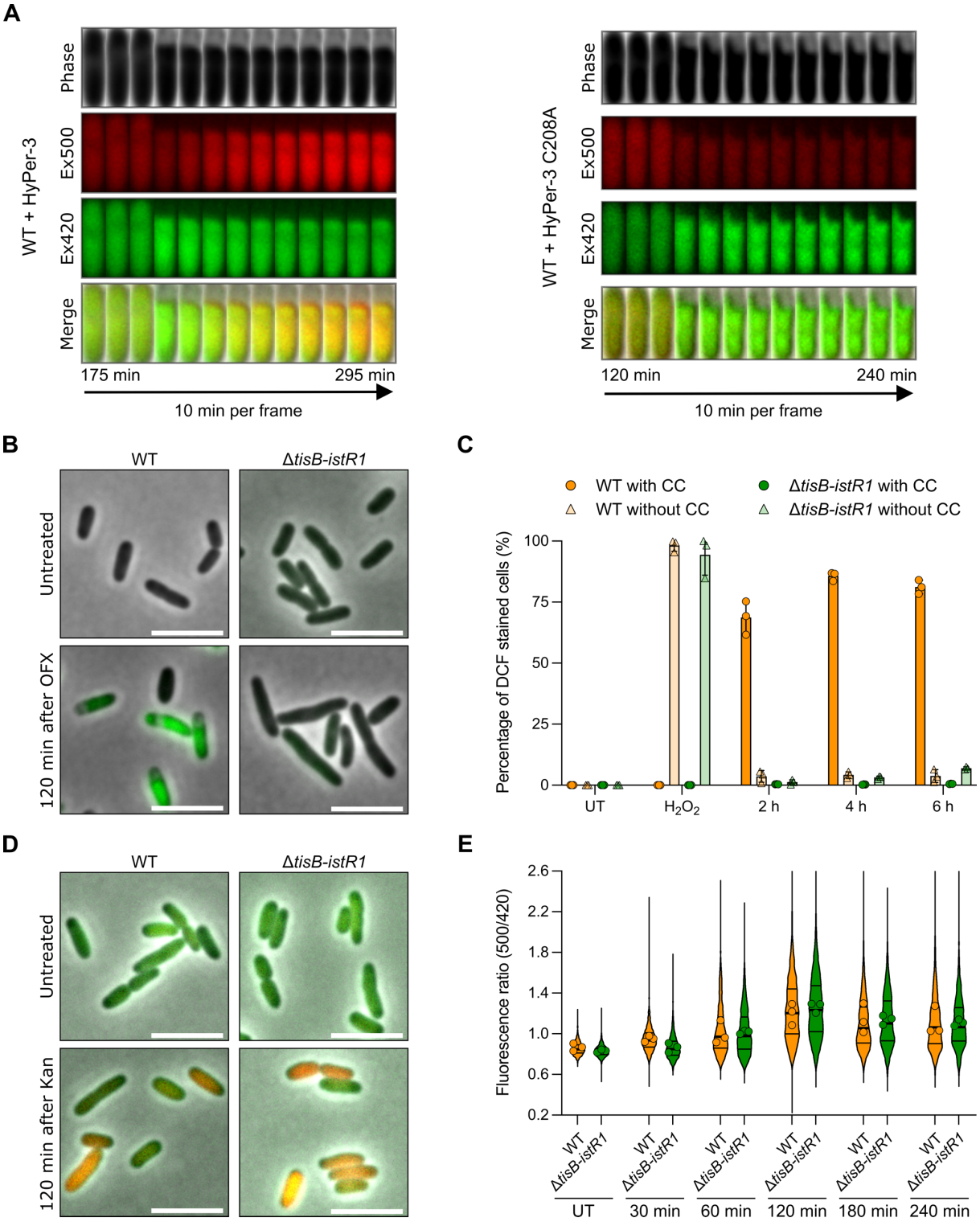

Figure S6: H_2O_2 production after OFX treatment is linked to cytoplasmic condensation

For all experiments, cells were grown in MOPS 0.4% glucose at 37°C to an OD_{600nm} ~ 0.3 and treated as described. Results are representative of 3 biological replicates. (A) Representative kymographs of WT cells containing HyPer-3 (left panel) and HyPer-3 C208A (right panel). Cells

were grown in microfluidic device for 60 min followed by perfusion with culture medium containing 5 µg/mL OFX for 360 min. Image acquisition was performed every 5 min. Phase contrast, fluorescence at 500 nm (red) and fluorescence at 420 nm (green) channels are shown as well as the merge of the fluorescence channels. (B) Representative images of fluorescent 2',7'-dichlorofluorescein (DCF)-staining in WT and Δ*tisB-istR1* cells before and 120 min after 5 µg/mL OFX treatment. At indicated times, samples were incubated with 2',7'-dichlorodihydrofluorescein diacetate (H_2DCFDA) for 40 min, spotted onto agarose pads and imaged. Scale bar = 5 µm. (C) Percentage of DCF-stained WT and Δ*tisB-istR1* cells with or without cytoplasmic condensation (CC) after OFX addition. Cells were treated and imaged as in (B). Positive control corresponds to cells treated with 100 mM H_2O_2. Between 116 and 1,106 cells were analyzed for each sample. The data points are mean ± SD. (D) Representative images of WT and Δ*tisB-istR1* cells containing the HyPer-3 reporter during kanamycin (Kan) treatment. Cells were treated with kanamycin (20 µg/mL) and spotted onto agarose pads 120 min after treatment. The merge of fluorescence channels (Ex. 500 nm (red), Ex. 420 nm (green)) and phase contrast is shown. (E) Intracellular H_2O_2 variations during Kan treatment. Cells were treated and imaged as in (D). At indicated times, the fluorescence ratio (500/420 nm) of individual WT (left panel) and Δ*tisB-istR1* cells (right panel) containing the HyPer-3 reporter was calculated. Between 206 and 1,449 cells were analyzed for each sample. The data points are mean of individual replicate (symbol), median (full line) ± quartiles (dashed line).

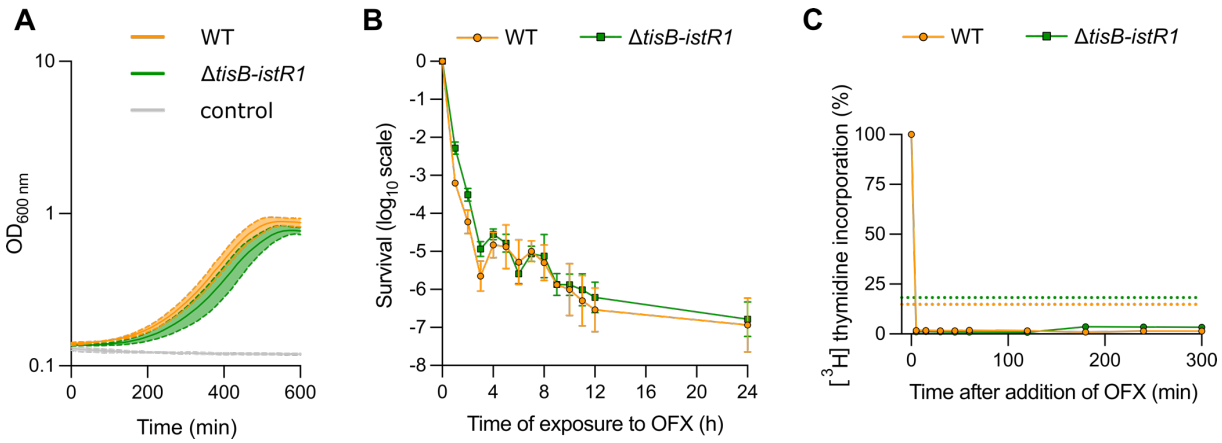

Figure S7: TisB does not contribute to OFX-mediated lethality

For all experiments, cells were grown in MOPS glucose 0.4% at 37°C to an OD_{600nm} ~ 0.3 and treated as described. Results are representative of 3 biological replicates. The data points are mean ± SD. (A) Growth curve of WT (orange line) and Δ*tisB-istR1* (green line) strains in MOPS-glucose 0.4% at 37°C. OD_{600nm} was measured every 15 min. (B) Survival of WT (orange) and Δ*tisB-istR1* (green) strains during 24 hours in the presence of OFX. At indicated times, culture samples were diluted and plated on LB agar plates. (C) Incorporation of radioactive [^{3}H]-thymidine during OFX treatment. WT and Δ*tisB-istR1* cells were treated with 5 µg/mL OFX. At indicated times, culture samples were incubated with radioactive [^{3}H]-thymidine for 5 min followed by trichloroacetic acid wash. Dashed line represents mean [^{3}H]-thymidine incorporation after 30 min MMC. The data points are mean ± SD.

Movie legends

Movie S1: Time-lapse movie of DNA compaction and cytoplasmic condensation induced by OFX in wild-type cells.

Related to figures 1A-C and S1A and S1D: Representative cells undergoing cytoplasmic condensation during OFX treatment. WT cells encoding a *hupA-mCherry* fusion and an IPTG-inducible periplasmic marker ^{SS}*dsbA-sfgfp* were grown in MOPS medium supplemented with

0.4% glucose and 250 µM IPTG at 37°C to an OD_{600nm} ~ 0.3. Cells were spotted onto agarose pads containing OFX (5 µg/mL) and IPTG (250 µM). Time-lapse image acquisition started 15 min after spotting with acquisition every 5 min. Phase contrast, mCherry (red) and GFP (green) channels are shown as well as the merge of the fluorescence channels. Yellow arrows indicate cells with cytoplasmic condensation. Scale bar = 5 µm.

Movie S2: Time-lapse movie of wild-type cells forming lateral and polar periplasmic expansion during OFX treatment

Related with Figure 1D and S1B-C: Representative cells forming lateral (left panel) or polar (right panel) periplasmic expansions. WT cells were grown in MOPS medium supplemented with 0.4% glucose at 37°C to an OD_{600nm} ~ 0.3. Cells were then spotted onto agarose pads containing OFX (5 µg/mL). Scale bar = 3 µm. Time-lapse image acquisition started 60 min after spotting with acquisition every 30 seconds.

Movie S3: Time-lapse movie of wild-type and ΔtisB-istR1 cells containing the HyPer-3 or HyPer-3 C208A reporters during OFX treatment

Related to Figure 5A-B and S6A. WT (upper panels) and Δ*tisB-istR1* (bottom panels) cells containing the HyPer-3 (left panels) or HyPer-3 C208A (right panels) were grown in the microfluidic device in MOPS 0.4% glucose at 37°C for 60 min. Cells were then perfused with culture medium containing OFX (5 µg/mL) for 360 min. Phase contrast, Ex. 500 nm (red) and Ex. 420 nm (green) channels are shown as well as the merge of the fluorescence channels. Image acquisition was performed every 15 min. Scale bar = 5 µm.

Supplementary tables

Strain	Genotype	Source or reference
MG1655 (BE10)	*E. coli* K-12 F- λ- *ilvG- rfb-50 rph-1 fnr*$^{+}$	Lab collection (*81)*
BE16	MG1655 *hupA-mCherry*-FRT-*kan*-FRT	P1(LY119) x BE10 to Kn^{r}
BE44	MG1655 *hupA-mCherry*-FRT-*kan*-FRT*, att*HKTB263 (P$_{lac}$::^{SS}*dsbA-sfgfp*)	P1(TB263) x BE16 to Ap^{r}
BE22	MG1655 *lexA3*(*Ind*$^{-}$), *malE300*::Tn10	Lab collection
BE48	MG1655 *hupA-mCherry*-FRT-*kan*-FRT*,* *lexA3*(*Ind*$^{-}$), *malE300*::Tn10	P1(BE22) x BE16 to Tet^{r}
BE61	MG1655 *hupA-mCherry*-FRT*,* Δ*tisB-istR1::*FRT-*kan*-FRT	P1(BE98) x BE181 to Kn^{r}
BE84	MG1655 Δ*tisB-istR::*FRT	Derivative from BE83, *kan* removed via pCP20
BE98	MG1655 Δ*tisB-istR::*FRT-*kan*-FRT	P1(CR*tisB-istR1*) x BE10 to Kn^{r}
BE181	MG1655, *hupA-mCherry*-FRT	Derivative from BE16, *kan* removed via pCP20
CR*tisB-istR1*	MG1655 Δ*tisB-istR::*FRT-*kan*-FRT	λred FRT-*kan*-FRT insertion replacing the *tisB-istR1* locus
TB263	*TB28, att*HKTB263 (P$_{lac}$::^{SS}*dsbA-sfgfp*)	From T. Bernhardt (*21*)
LY123	MS388 *hupA-mCherry-FRT-kan-FRT*	From C. Lesterlin (*89*)

Table S1. Strains

Plasmid	Description	Source or reference
pCP20	FLP expression plasmid	(*82*)
HyPer-3	pBeloBAC11 derivative encoding the *E. coli* optimized H_2O_2 sensor Hyper-3 under the control of the *proDp-0034b* region	Lab collection
HyPer-3 C208A	HyPer-3 with cysteine 208 substituted by alanine	This work
p*katG-gfp$_{mut2}$*	pUA66 derivative, pSC101 origin, *katG* promoter region cloned upstream of the *gfp$_{mut2}$* gene	(*44*)
pKD4	Carries *FRT-kan-FRT* used for λred integration	(*82*)
pKD46	Plasmid for λred recombination	(*82*)
pNF02	oriF *cat* λt1ter-proDp-*mScarlet-I*-T7TE*luxI*A	Lab collection (*90*)
pNF02-EV	pNF02 derivative single copy plasmid without proDp-*mScarlet-I*	This work
pNF02-*tisB*	pNF02 derivative containing the *tisB* gene under the control of its native promoter	This work
pNF02-*tisB-istR1*	pNF02 derivative containing the *tisB-istR1* locus	This work

pHluorin2	pBeloBAC11 derivative encoding the *E. coli* optimized pH sensor pHluorin2 under the control of the *proDp-0034b* region	Lab collection
pUA66-*pistR1-tisB-gfp*$_{mut2}$	pSC101 origin, *istR1-tisB* promoter region cloned upstream of the *gfp*$_{mut2}$ gene	From I. Matic (*35*)

Table S2. Plasmids

Primer	Sequence (5'-3')	Construction
P1	CAATATTTATACAAGCACAGCTTTACAGGGGAGACA ATGGAAAATTTTTCATTCCGGGGATCCGTCGACC	λred *FRT-kan-FRT* insertion at the *istR1-tisB locus*. PCR on pKD4
P2	TGTTTAGCGGCAGAATATGTAAACAAAAGCGGCAA TAAATGTTGCCGGGATGT AGGCTGGAGCTGCTTCG	
P3	GATGGCGCAGTTGGTAGTAGTTTTGCGTTGAGCAT G	Verification of *FRT-kan-FRT* insertion at the *istR1-tisB* locus
P4	CTTACAAAAATGGTGTGGCAGCGAAAACCCGCAAC C	
P5	ACGCGTAAAAAATTAGCGCAAGAAGACAAAAATC	Construction of the pNF02-EV plasmid. Amplification of pNF02 without proDp-*mScarlet-I*. PCR on pNF02
P6	GTGCACCTCTAGTATCACACTGGCTC	
P7	TGATCGAACGCGTAAAAAATTAGCGCA	pNF02-*tisB* and pNF02-*tisB-istR1* plasmids constructed by Gibson assembly. (P7-P9) for cloning *tisB* gene and *tisB-istR1* locus (P8-P9) in pNF02-EV plasmid
P8	GTGCGGGTTGGTGTGCACCTCTAGTATCACACTGGC TC	
P9	TTGTTATCTGCAACGCGTAAAAAATTAGCGCAAG	
P10	TTTTACGCGTTCGATCACAGTTTGCGTTTT	PCR amplification of *tisB* gene (P10-P11) and *tisB-istR1* locus (P11-P12) for construction of pNF02-*tisB* and pNF02-*tisB-istR1* plasmids by Gibson assembly with pNF02-EV
P11	CTAGAGGTGCACACCAACCCGCACGCTAAAT	
P12	AATTTTTTACGCGTTGCAGATAACAAAAAACCCC	
P13	AGAGCATTAGCGCAAGGTG	Sequencing of pNF02-*tisB* and pNF02-*tisB-istR1* plasmids
P14	ATTGTCGATCAGACTATCAGC	
P15	GGGCGGATGAAGATACACACTTCCG	Substitution of the cysteine 208 by alanine. PCR on HyPer-3
P16	CGGCTTCAAACGCGAAACCGGTGCC	
P17	GGTGATGTCGGCGATATAGG	PCR amplification of pHluorin2 fragment on pET28- XbaI-34b-pHluorin2-N3-NotI
P18	GCTAGTTATTGCTCAGCGG	

Table S3. PCR primers used for strain and plasmid construction

Chemically synthesized fragment by IDT, Inc.	Sequence (5'-3')	Construction

proDp-RBS0034b	CACAGCTAACACCACGTCGTCCCTATCTGCTGCCCTAGGTCTATG AGTGGTTGCTGGATAACTTTACGGGCATGCATAAGGCTCGTATAA TATATTCAGGGAGACCACAACGGTTTCCCTCTACAAATAATTTTGT TTAACTTTTACTAGAGAAAGAGGAGAAA	HyPer-3 and pHluorin2
MluI-34b-6His-HyPer-3-N1-ApaLI	GCTCCGACGCGTTACTAGAGAAAGAGGAGAAAGCTAGCATGAG AGGTTCGCACCATCATCACCACCACGGATCGGAAATGGCAAGCC AGCAGGGCGAGACGATGTCGGGACCGTTGCACATAGGTTTGAT TCCCACAGTTGGACCGTACCTGCTACCGCATATTATCCCTATGCTG TACCAGACCTTTCCAAAGCTGGAAATGTATCTGCATGAGGCACA GACCCACCAGTTACTGGCGCAACTGGACAGCGGCAAACTCGATT GCGTGATCCTCGCACTGGTGAAAGAGAGCGAAGCATTCATTGAA GTGCCGTTGTTTGATGAGCCAATGTTGCTGGCTATCTATGAAGAT CACCCGTGGGCGAACCGCGAATGCGTACCGATGGCCGATCTGGC AGGCGAAAAACTGCTGATGCTGGAAGATGGTCACTGTTTGCGC GATCAGGCAATGTCCGCCGGCTACAACAGCGACAACGTCTATATC ATGGCCGACAAGCAGAAGAACGGCATCAAGGCCAACTTCAAGA TCCGCCACAACGTCGAAGACGGCAGCGTGCAGCTCGCCGACCA CTACCAGCAGAACACCCCCATCGGCGACGGCCCCGTGCTGCTGC CCGACAACCACTACCTGAGCTTCCAGTCCGTCCTGAGCAAAGAC CCCAACGAGAAGCGCGATCACATGGTCCTGCTGGAGTTCGTGAC CGCCGCCGGGATCACTCTCGGCATGGACGAGCTGTACAACGTG GATGGCGGTAGCGGTGGCACCGGCAGCAAGGGCGAGGAGCTG TTCACCGGGGTGGTGCCCATCCTGGTCGAGCTGGACGGCGACG TAAACGGCCACAAGTTCAGCGTGTCCGGCGAGGGTGAGGGCG ATGCCACCTACGGTAAGCTGACCCTGAAGCTGATCTGCACCACC GGCAAGCTGCCCGTGCCCTGGCCCACCTTGGTGACCACCCTCGG CTACGGCCTGAAGTGCTTCGCCCGCTACCCCGACCACATGAAGC AGCACGACTTCTTTAAGTCCGCCATGCCCGAAGGCTACGTCCAG GAGCGCACCATCTTCTTCAAAGACGACGGTAACTACAAGACCCG CGCCGAGGTGAAGTTCGAGGGCGACACCCTGGTGAACCGCATC GAGCTGAAGGGCATCGGCTTCAAGGAGGACGGCAACATCCTGG GGCACAAGCTGGAGTACAACGGCACCGGTTTCTGTTTTGAAGC CGGGGCGGATGAAGATACACACTTCCGCGCGACCAGCCTGGAA ACTCTGCGCAACATGGTGGCGGCAGGTAGCGGGATCACTTTACT GCCAGCGCTGGCTGTGCCGCCGGAGCGCAAACGCGATGGGGTT GTTTATCTGCCGTGCATTAAGCCGGAACCACGCCGCACTATTGGT CTGGTTTATCGTCCTGGCTCACCGCTGCGCAGCCGCTATGAGCA GCTGGCAGAGGCCATCCGCGCAAGAATGGATGGCCATTTCGATA AAGTTTTAAAACAGGCGGTTTAATGACTAAGTAAGGCGCCACTG GTGCACCTCTAGTATCAC	HyPer-3
XbaI-34b-pHluorin2-N3-NotI	GCGGATAACAATTCCCCTCTAGAGGGAGACCACAACGGTTTCCC TCTACAAATAATTTTGTTTAACTTTTACTAGAGAAAGAGGAGAAA GCTAGCATGGTTTCAAAAGGCGAAGAACTATTTACCGGCGTAGT GCCCATTCTGGTTGAACTGGATGGCGATGTTAACGGTCATAAATT CTCGGTAAGCGGCGAAGGCGAAGGCGATGCCACCTATGGCAAA CTGACCCTGAAATTCATCTGCACCACCGGTAAACTGCCGGTGCC GTGGCCGACGCTGGTCACCACCCTGTCGTATGGCGTGCAGTGCT	pHluorin2

	TTAGCCGCTATCCGGATCACATGAAACAGCACGATTTCTTTAAAT CCGCCATGCCCGAAGGCTATGTCCAGGAACGCACCATTTTCTTCA AAGATGATGGCAACTACAAAACCCGCGCCGAAGTGAAATTCGA AGGCGATACCCTGGTGAATCGCATTGAACTGAAAGGCATTGATT TTAAAGAGGATGGCAACATCCTGGGCCATAAACTGGAATATAACT ACAACGAACATCTGGTGTATATCATGGCCGATAAACAAAAAAAC GGCACCAAAGCTATCTTCCAGGTGCATCATAACATCGAAGATGGC AGCGTGCAGCTGGCGGATCACTATCAGCAGAACACCCCGATTGG CGATGGCCCGGTGCTGCTGCCGGATAACCATTATCTGCATACCCA GTCGGCGCTGTCGAAAGATCCGAACGAAAAACGCGATCACATG GTGCTGCTGGAATTTGTCACCGCCGCCGGTATCACCCATGGCATG GACGAACTGTATAAATAATGACTAAGTAAGGCGCCACTGGTGCA CCTCTAGTATGCGGCCGCACTCGAGCACCA	

Table S4. DNA sequences used for the optimization of the HyPer-3 and pHluorin2 reporters

Fluorescent reporter or dye	**LED/filter (ex, em)**	**Power (%)/ exposure (ms)**
HU-mCherry	555 nm LED/00 Nil red (530-585 ex, 615LP em)	50/300
^{SS}DsbA-GFP	475 nm LED/38HE (450-490 ex, 500-550 em)	10/300
tisB transcriptional fusion	475 nm LED/38HE (450-490 ex, 500-550 em)	5/10
pHluorin2	430 nm LED/custom filter (405/20 ex, 535/50 em) 475 nm LED/38HE (450-90 ex, 500-550 em)	30/500 5/600
HyPer-3 and pHyPer-3 C208A	430 nm LED/custom filter (405/20 ex, 525/30 em) 511 nm LED/46YFP (490-510 ex, 520-550 em)	20/600 80/500
Propidium iodide	555 nm LED/00 Nil red (530-585 ex, 615LP em)	5/100
$DiBAC_4(3)$	475 nm LED/38HE (450-490 ex, 500-550 em)	10/100
Syto9	475 nm LED/38HE (450-490 ex, 500-550 em)	5/100
H_2DCFDA	475 nm LED/38HE (450-490 ex, 500-550 em)	50/150

Table S5: Microscopy parameters

Supplementary notes

Excitation spectrum and calibration of pHluorin2 for intracellular pH quantification

Properties of the pHluorin2 reporter are represented in Figure S8A.

Excitation spectra: Excitation spectrum of WT cells containing the plasmid-encoded pHluorin2 reporter was measured using the SpectraMax i3 (Figure S8B). Fifteen mL of culture at OD_{600nm} ~ 0.3 grown in MOPS 0.4% glucose were centrifuged at 3,275 g for 15 minutes at 20°C and resuspended in saline solution (pH 6.5). Ninety µL of MOPS 0.4% glucose adjusted to different pH (5.5, 6.5, 7.5 or 8.5) supplemented with and without 40 mM sodium benzoate was added to a 96-well black border clear flat bottom plate and pre-warmed to 37°C. Ten µL of cell suspension were added to each well. Fluorescence excitation spectra at emission of 535 nm was recorded using SpectraMax i3. Excitation scans were performed between wavelength 380 nm to 510 nm in 2 nm-steps and with the emission set at 535 ± 15 nm. The background from non-fluorescent cells was subtracted from the signal. Based on the excitation spectrum, excitation wavelengths of 420 nm and 470 nm were selected for the ratiometric analysis of intracellular pH.

Calibration: WT cells containing the plasmid-encoded pHluorin2 reporter were grown overnight (16-18 h) in MOPS 0.4% glucose adjusted to different pH (5.5, 6.5, 7.5 or 8.5). Cultures were diluted to an OD_{600nm} of 0.01 in the corresponding media and grown at 37°C to an OD_{600nm} of 0.3. Cells were loaded into a microfluidic plate and perfused for 1 hours at 37°C in the corresponding pH-adjusted media, followed by a perfusion of 50 min with 40 mM sodium benzoate. Fluorescence microscopy was performed with excitation wavelengths of 420 nm and 470 nm and emission was measured at 535 nm. Fluorescence intensity analysis was performed using the MicrobeJ plug-in and the fluorescence ratio (470/420 nm) was calculated (Figure S8C).

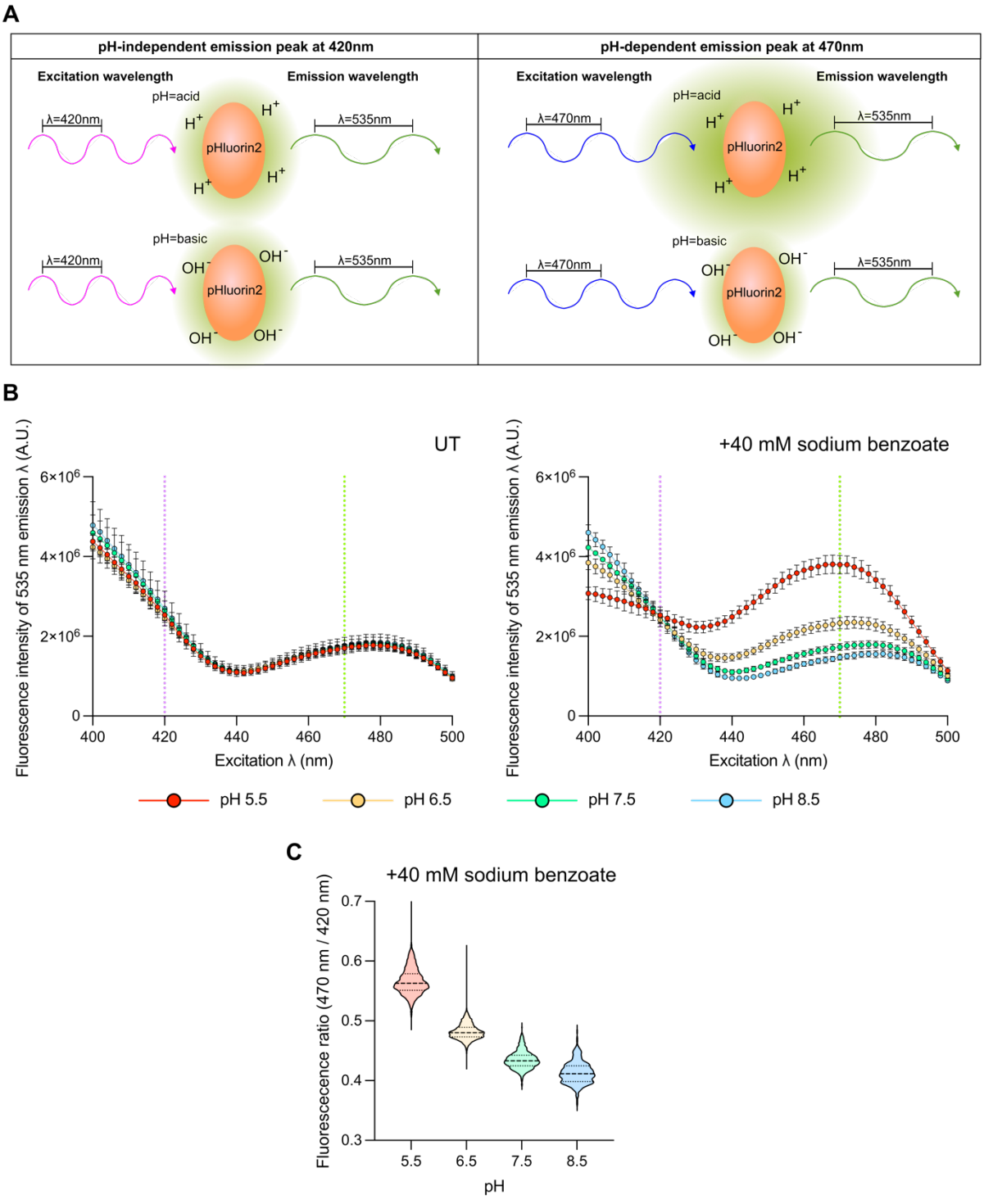

Figure S8: Characterization of the pHluorin2 reporter

(A) Schematic representation of pHluorin2 properties. (B) pHluorin2 excitation spectrum at different pH. WT cells containing the plasmid-encoded pHluorin2 reporter were grown in MOPS 0.4% glucose adjusted to different pH at 37°C to an OD_{600nm} ~ 0.3. Cells were centrifuged

and resuspended in their corresponding pH-adjusted MOPS 0.4% glucose medium containing or not 40 mM sodium benzoate. Fluorescence excitation spectrum at emission wavelength of 535 nm was measured using SpectraMax i3. Results are representative of 3 biological replicates. The data points are mean ± SD. (C) Validation of pHluorin2 in the microfluidic system. Wild-type cells containing the plasmid-encoded pHluorin2 reporter were grown in the microfluidic device in MOPS 0.4% glucose adjusted to different pH at 37°C for 60 min followed by perfusion of 40 mM sodium benzoate. Fifteen min later, pHluorin2 was excited using 420 nm and 470 nm and emission wavelength was measured at 535 nm. Results are representative of 3 biological replicates. At total of at least 500 cells analyzed. The data points are median (full line) ± quartiles (dashed line).

Excitation spectra of pHyPer-3 and pHyPer-3 C208A in presence of H_2O_2 or at different pH

Properties of the HyPer-3 and HyPer-3 C208A reporters are represented in Figure S9A, upper panel.

Excitation spectra in presence of H_2O_2: Excitation spectra of WT cells containing the plasmid-encoded HyPer-3 or HyPer-3 C208A reporter were measured using the SpectraMax i3. Fifteen mL of culture at OD_{600nm} ~ 0.3 grown in MOPS 0.4% glucose were centrifuged at 3,275 g for 15 min at 20°C and resuspended in saline solution (pH 6.5). Ninety µL of MOPS 0.4% glucose supplemented with 0 µM, 50 µM, 100 µM, 500 µM, 1 mM or 10 mM H_2O_2 were added to a 96-well black border clear flat bottom plate and pre-warmed to 37°C. Ten µL of cell suspension were added to each well. Fluorescence excitation spectra at emission of 535 nm were recorded using SpectraMax i3. Excitation scans were performed between wavelength 380 nm to 510 nm in 2 nm-steps and with the emission set at 535 ± 15 nm. The background from non-fluorescent

cells was subtracted from the signal. Based on the excitation spectrum, excitation wavelengths of 420 nm and 500 nm were selected for the ratiometric analysis of intracellular H_2O_2 levels.

Excitation spectra at different pH: Excitation spectra of WT cells containing the plasmid-encoded HyPer-3 or HyPer-3-C208A reporter were measured using the SpectraMax i3. Fifteen mL of culture at OD_{600nm} ~ 0.3 grown in MOPS 0.4% glucose were centrifuged at 3,275g for 15 minutes at 20°C and resuspended in saline solution (pH 6.5). Ninety µL of MOPS 0.4% glucose adjusted to different pH (5.5, 6.5, 7.5 or 8.5) supplemented with and without 40mM sodium benzoate was added to a 96-well black border clear flat bottom well plate and pre-warmed to 37°C. Ten µL of cell suspension were added to each well. Fluorescence excitation spectra at emission of 535 nm was performed using SpectraMax i3. Excitation scans were performed between wavelength 380 nm to 510 nm in 2 nm-steps and with the emission set at 535 nm ± 15. The background from non-fluorescent cells was subtracted from the signal (Figure S9B).

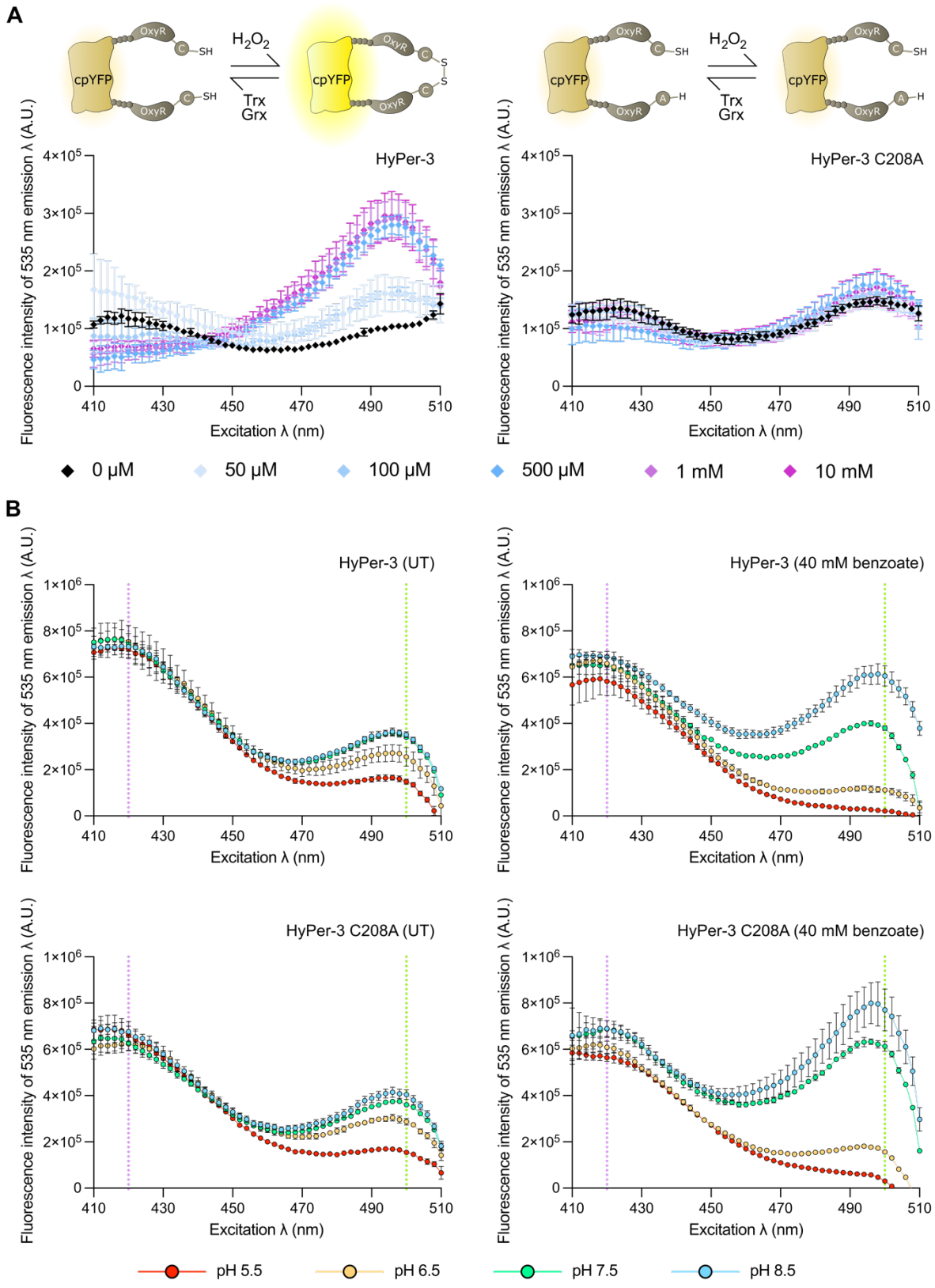
A
cpYFP
OxyR
SH
H_2O_2
Trx
Grx
HyPer-3
HyPer-3 C208A
Fluorescence intensity of 535 nm emission λ (A.U.)
Excitation λ (nm)
0 μM
50 μM
100 μM
500 μM
1 mM
10 mM
B
HyPer-3 (UT)
HyPer-3 (40 mM benzoate)
HyPer-3 C208A (UT)
HyPer-3 C208A (40 mM benzoate)
pH 5.5
pH 6.5
pH 7.5
pH 8.5

Figure S9: Characterization of HyPer-3 and HyPer-C208A reporters

(A) Schematic representation of HyPer-3 and HyPer-C208A properties (upper panel) and fluorescence excitation spectrum of HyPer-3 and HyPer-C208A in presence of different doses of H_2O_2 (bottom panel). WT cells containing the plasmid-encoded HyPer-3 (left) or HyPer-C208A (right) reporter were grown in MOPS 0.4% glucose adjusted to an OD_{600nm} ~ 0.3. Cultures were diluted to an OD_{600nm} of 0.01 in PBS and H_2O_2 was added at the following concentrations: 50 µM, 100 µM, 500 µM, 1 mM and 10 mM. The untreated (0 µM) condition corresponds to a culture without exogenous H_2O_2. Fluorescence excitation spectrum at emission wavelength of 535 nm was measured using Spectramax i3. Results are representative of 3 biological replicates. The data points are mean ± SD. (B) Fluorescence excitation spectrum of the HyPer-3 and HyPer-C208A biosensors at different pH. Wild-type cells containing the plasmid-encoded HyPer-3 or HyPer-C208A reporter were grown in MOPS 0.4% glucose adjusted to different pH at 37°C to an OD_{600nm} ~ 0.3. Cells were centrifuged and resuspended in their corresponding pH-adjusted MOPS 0.4% glucose containing or not 40 mM sodium benzoate. Fluorescence excitation spectrum at emission wavelength of 535 nm was measured using Spectramax i3. Results are representative of 3 biological replicates. The data points are mean ± SD.

REFERENCES AND NOTES

1. A. Gutierrez, J. M. Stokes, I. Matic, Our evolving understanding of the mechanism of quinolones. *Antibiotics (Basel)* **7**, 32 (2018).

2. M. A. Kohanski, D. J. Dwyer, J. J. Collins, How antibiotics kill bacteria: From targets to networks. *Nat. Rev. Microbiol.* **8**, 423–435 (2010).

3. E. M. Darby, E. Trampari, P. Siasat, M. S. Gaya, I. Alav, M. A. Webber, J. M. A. Blair, Molecular mechanisms of antibiotic resistance revisited. *Nat. Rev. Microbiol.* **21**, 280–295 (2023).

4. M. A. Kohanski, D. J. Dwyer, B. Hayete, C. A. Lawrence, J. J. Collins, A common mechanism of cellular death induced by bactericidal antibiotics. *Cell* **130**, 797–810 (2007).

5. D. J. Dwyer, M. A. Kohanski, B. Hayete, J. J. Collins, Gyrase inhibitors induce an oxidative damage cellular death pathway in *Escherichia coli*. *Mol. Syst. Biol.* **3**, 91 (2007).

6. M. A. Lobritz, P. Belenky, C. B. M. Porter, A. Gutierrez, J. H. Yang, E. G. Schwarz, D. J. Dwyer, A. S. Khalil, J. J. Collins, Antibiotic efficacy is linked to bacterial cellular respiration. *Proc. Natl. Acad. Sci. U.S.A.* **112**, 8173–8180 (2015).

7. P. Belenky, J. D. Ye, C. B. M. Porter, N. R. Cohen, M. A. Lobritz, T. Ferrante, S. Jain, B. J. Korry, E. G. Schwarz, G. C. Walker, J. J. Collins, Bactericidal antibiotics induce toxic metabolic perturbations that lead to cellular damage. *Cell Rep.* **13**, 968–980 (2015).

8. Y. Hong, Q. Li, Q. Gao, J. Xie, H. Huang, K. Drlica, X. Zhao, Reactive oxygen species play a dominant role in all pathways of rapid quinolone-mediated killing. *J. Antimicrob. Chemother.* **75**, 576–585 (2020).

9. X. Wang, X. Zhao, M. Malik, K. Drlica, Contribution of reactive oxygen species to pathways of quinolone-mediated bacterial cell death. *J. Antimicrob. Chemother.* **65**, 520–524 (2010).

10. F. Wong, J. M. Stokes, B. Cervantes, S. Penkov, J. Friedrichs, L. D. Renner, J. J. Collins, Cytoplasmic condensation induced by membrane damage is associated with antibiotic lethality. *Nat. Commun.* **12**, 2321 (2021).

11. L. A. Simmons, J. J. Foti, S. E. Cohen, G. C. Walker, The SOS regulatory network. *EcoSal Plus.* **3**, 10.1128/ecosalplus.5.4.3 (2008).

12. I. Erill, S. Campoy, J. Barbé, Aeons of distress: An evolutionary perspective on the bacterial SOS response. *FEMS Microbiol. Rev.* **31**, 637–656 (2007).

13. Z. Baharoglu, D. Mazel, SOS, the formidable strategy of bacteria against aggressions. *FEMS Microbiol. Rev.* **38**, 1126–1145 (2014).

14. I. Matic, F. Taddei, M. Radman, Survival versus maintenance of genetic stability: A conflict of priorities during stress. *Res. Microbiol.* **155**, 337–341 (2004).

15. T. Dörr, K. Lewis, M. Vulić, SOS response induces persistence to fluoroquinolones in Escherichia coli. *PLOS Genet.* **5**, e1000760 (2009).

16. F. Goormaghtigh, L. Van Melderen, Single-cell imaging and characterization of *Escherichia coli* persister cells to ofloxacin in exponential cultures. *Sci. Adv.* **5**, eaav9462 (2019).

17. K. G. Völzing, M. P. Brynildsen, Stationary-phase persisters to ofloxacin sustain DNA damage and require repair systems only during recovery. *MBio* **6**, e00731–00715 (2015).

18. J. M. Diver, R. Wise, Morphological and biochemical changes in *Escherichia coli* after exposure to ciprofloxacin. *J. Antimicrob. Chemother.* **18**, 31–41 (1986).

19. T. J. Dougherty, J. J. Saukkonen, Membrane permeability changes associated with DNA gyrase inhibitors in Escherichia coli. *Antimicrob. Agents Chemother.* **28**, 200–206 (1985).

20. J. K. Fisher, A. Bourniquel, G. Witz, B. Weiner, M. Prentiss, N. Kleckner, Four-dimensional imaging of *E. coli* nucleoid organization and dynamics in living cells. *Cell* **153**, 882–895 (2013).

21. T. Dinh, T. G. Bernhardt, Using superfolder green fluorescent protein for periplasmic protein localization studies. *J. Bacteriol.* **193**, 4984–4987 (2011).

22. I. Odsbu, K. Skarstad, DNA compaction in the early part of the SOS response is dependent on RecN and RecA. *Microbiology (Reading).* **160**, 872–882 (2014).

23. C. Lesterlin, G. Ball, L. Schermelleh, D. J. Sherratt, RecA bundles mediate homology pairing between distant sisters during DNA break repair. *Nature* **506**, 249–253 (2014).

24. E. Vickridge, C. Planchenault, C. Cockram, I. G. Junceda, O. Espéli, Management of *E. coli* sister chromatid cohesion in response to genotoxic stress. *Nat. Commun.* **8**, 14618 (2017).

25. J. W. Little, J. E. Harper, Identification of the lexA gene product of Escherichia coli K-12. *Proc. Natl. Acad. Sci. U.S.A.* **76**, 6147–6151 (1979).

26. L. L. Lin, J. W. Little, Isolation and characterization of noncleavable (Ind-) mutants of the LexA repressor of Escherichia coli K-12. *J. Bacteriol.* **170**, 2163–2173 (1988).

27. C. Unoson, E. G. H. Wagner, A small SOS-induced toxin is targeted against the inner membrane in Escherichia coli. *Mol. Microbiol.* **70**, 258–270 (2008).

28. P. A. Gurnev, R. Ortenberg, T. Dörr, K. Lewis, S. M. Bezrukov, Persister-promoting bacterial toxin TisB produces anion-selective pores in planar lipid bilayers. *FEBS Lett.* **586**, 2529–2534 (2012).

29. T. Steinbrecher, S. Prock, J. Reichert, P. Wadhwani, B. Zimpfer, J. Bürck, M. Berditsch, M. Elstner, A. S. Ulrich, Peptide-lipid interactions of the stress-response peptide TisB that induces bacterial persistence. *Biophys. J.* **103**, 1460–1469 (2012).

30. B. A. Berghoff, M. Hoekzema, L. Aulbach, E. G. H. Wagner, Two regulatory RNA elements affect TisB-dependent depolarization and persister formation. *Mol. Microbiol.* **103**, 1020–1033 (2017).

31. J. Vogel, L. Argaman, E. G. H. Wagner, S. Altuvia, The small RNA IstR inhibits synthesis of an SOS-induced toxic peptide. *Curr. Biol.* **14**, 2271–2276 (2004).

32. F. Darfeuille, C. Unoson, J. Vogel, E. G. H. Wagner, An antisense RNA inhibits translation by competing with standby ribosomes. *Mol. Cell* **26**, 381–392 (2007).

33. E. G. H. Wagner, C. Unoson, The toxin-antitoxin systemtisB-istR1. *RNA Biol.* **9**, 1513–1519 (2012).

34. C. Romilly, A. Lippegaus, E. G. H. Wagner, An RNA pseudoknot is essential for standby-mediated translation of the tisB toxin mRNA in *Escherichia coli*. *Nucleic Acids Res.* **48**, 12336–12347 (2020).

35. W.-L. Su, M.-F. Bredèche, S. Dion, J. Dauverd, B. Condamine, A. Gutierrez, E. Denamur, I. Matic, TisB protein protects Escherichia coli cells suffering massive DNA damage from environmental toxic compounds. *MBio* **13**, e0038522 (2022).

36. E. Mulder, C. L. Woldringh, Plasmolysis bays in Escherichia coli: Are they related to development and positioning of division sites? *J. Bacteriol.* **175**, 2241–2247 (1993).

37. H. Shi, C. S. Westfall, J. Kao, P. D. Odermatt, S. E. Anderson, S. Cesar, M. Sievert, J. Moore, C. G. Gonzalez, L. Zhang, J. E. Elias, F. Chang, K. C. Huang, P. A. Levin, Starvation induces shrinkage of the bacterial cytoplasm. *Proc. Natl. Acad. Sci. U.S.A.* **118**, e2104686118 (2021).

38. T. Kogoma, T. A. Torrey, M. J. Connaughton, Induction of UV-resistant DNA replication in Escherichia coli: Induced stable DNA replication as an SOS function. *Mol. Gen. Genet.* **176**, 1–9 (1979).

39. D. Edelmann, B. A. Berghoff, Type I toxin-dependent generation of superoxide affects the persister life cycle of Escherichia coli. *Sci. Rep.* **9**, 14256 (2019).

40. D. S. Adams, M. Levin, Measuring resting membrane potential using the fluorescent voltage reporters DiBAC4(3) and CC2-DMPE. *Cold Spring Harb. Protoc.* **2012**, 459–464 (2012).

41. T. A. Krulwich, G. Sachs, E. Padan, Molecular aspects of bacterial pH sensing and homeostasis. *Nat. Rev. Microbiol.* **9**, 330–343 (2011).

42. M. J. Mahon, pHluorin2: An enhanced, ratiometric, pH-sensitive green florescent protein. *ABB.* **02**, 132–137 (2011).

43. D. Edelmann, B. A. Berghoff, Type I toxin-dependent generation of superoxide affects the persister life cycle of Escherichia coli. *Sci. Rep*. **9**, 14256 (2019).

44. O. K. Silander, N. Nikolic, A. Zaslaver, A. Bren, I. Kikoin, U. Alon, M. Ackermann, A genome-wide analysis of promoter-mediated phenotypic noise in *Escherichia coli*. *PLOS Genet.* **8**, e1002443 (2012).

45. P. C. Loewen, J. Switala, Purification and characterization of catalase HPII from *Escherichia coli* K12. *Biochem. Cell Biol.* **64**, 638–646 (1986).

46. A. Sen, J. A. Imlay, How microbes defend themselves from incoming hydrogen peroxide. *Front. Immunol.* **12**, 667343 (2021).

47. C. J. Willmott, S. E. Critchlow, I. C. Eperon, A. Maxwell, The complex of DNA gyrase and quinolone drugs with DNA forms a barrier to transcription by RNA polymerase. *J. Mol. Biol.* **242**, 351–363 (1994).

48. D. S. Bilan, L. Pase, L. Joosen, A. Y. Gorokhovatsky, Y. G. Ermakova, T. W. J. Gadella, C. Grabher, C. Schultz, S. Lukyanov, V. V. Belousov, HyPer-3: A genetically encoded H(2)O(2) probe with improved performance for ratiometric and fluorescence lifetime imaging. *ACS Chem. Biol.* **8**, 535–542 (2013).

49. D. J. Dwyer, P. A. Belenky, J. H. Yang, I. C. MacDonald, J. D. Martell, N. Takahashi, C. T. Y. Chan, M. A. Lobritz, D. Braff, E. G. Schwarz, J. D. Ye, M. Pati, M. Vercruysse, P. S. Ralifo, K. R. Allison, A. S. Khalil, A. Y. Ting, G. C. Walker, J. J. Collins, Antibiotics induce redox-related physiological alterations as part of their lethality. *Proc. Natl. Acad. Sci. U.S.A.* **111**, E2100–2109 (2014).

50. S. R. Martínez, A. M. Durantini, M. C. Becerra, G. Cosa, Real-time single-cell imaging reveals accelerating lipid peroxyl radical formation in Escherichia coli triggered by a fluoroquinolone antibiotic. *ACS Infect Dis.* **6**, 2468–2477 (2020).

51. W. A. Goss, W. H. Deitz, T. M. Cook, Mechanism of action of nalidixic acid on Escherichia coli II. Inhibition of deoxyribonucleic acid synthesis. *J. Bacteriol.* **89**, 1068–1074 (1965).

52. J. R. Pohlhaus, K. N. Kreuzer, Norfloxacin-induced DNA gyrase cleavage complexes block Escherichia coli replication forks, causing double-stranded breaks in vivo. *Mol. Microbiol.* **56**, 1416–1429 (2005).

53. A. Maxwell, The molecular basis of quinolone action. *J. Antimicrob. Chemother.* **30**, 409–414 (1992).

54. M. T. Howard, S. H. Neece, S. W. Matson, K. N. Kreuzer, Disruption of a topoisomerase-DNA cleavage complex by a DNA helicase. *Proc. Natl. Acad. Sci. U.S.A.* **91**, 12031–12035 (1994).

55. L. M. Wentzell, A. Maxwell, The complex of DNA gyrase and quinolone drugs on DNA forms a barrier to the T7 DNA polymerase replication complex. *J. Mol. Biol.* **304**, 779–791 (2000).

56. V. Schneider, P. Wadhwani, J. Reichert, J. Bürck, M. Elstner, A. S. Ulrich, T. Kubař, Tetrameric charge-zipper assembly of the TisB peptide in membranes-computer simulation and experiment. *J. Phys. Chem. B* **123**, 1770–1779 (2019).

57. S. L. Grage, S. Afonin, S. Kara, G. Buth, A. S. Ulrich, Membrane thinning and thickening induced by membrane-active amphipathic peptides. *Front. Cell Dev. Biol.* **4**, 65 (2016).

58. G. V. Smirnova, A. V. Tyulenev, N. G. Muzyka, M. A. Peters, O. N. Oktyabrsky, Ciprofloxacin provokes SOS-dependent changes in respiration and membrane potential and causes alterations in the redox status of Escherichia coli. *Res. Microbiol.* **168**, 64–73 (2017).

59. A. M. Brauer, H. Shi, P. A. Levin, K. C. Huang, Physiological and regulatory convergence between osmotic and nutrient stress responses in microbes. *Curr. Opin. Cell Biol.* **81**, 102170 (2023).

60. P. A. Swenson, R. L. Schenley, Evidence for the control of respiration by DNA in ultraviolet-irradiated Escherichia coli B-r cells. *Mutat. Res.* **9**, 443–453 (1970).

61. P. A. Swenson, R. L. Schenley, Evidence relating cessation of respiration, cell envelope changes, and death in ultraviolet-irradiated *Escherichia coli* B/r cells. *J. Bacteriol.* **117**, 551–559 (1974).

62. Y. Liu, J. A. Imlay, Cell death from antibiotics without the involvement of reactive oxygen species. *Science* **339**, 1210–1213 (2013).

63. B. Ezraty, A. Vergnes, M. Banzhaf, Y. Duverger, A. Huguenot, A. R. Brochado, S.-Y. Su, L. Espinosa, L. Loiseau, B. Py, A. Typas, F. Barras, Fe-S cluster biosynthesis controls uptake of aminoglycosides in a ROS-less death pathway. *Science* **340**, 1583–1587 (2013).

64. I. Keren, Y. Wu, J. Inocencio, L. R. Mulcahy, K. Lewis, Killing by bactericidal antibiotics does not depend on reactive oxygen species. *Science* **339**, 1213–1216 (2013).

65. L. C. Seaver, J. A. Imlay, Are respiratory enzymes the primary sources of intracellular hydrogen peroxide? *J. Biol. Chem.* **279**, 48742–48750 (2004).

66. S. Korshunov, J. A. Imlay, Two sources of endogenous hydrogen peroxide in Escherichia coli. *Mol. Microbiol.* **75**, 1389–1401 (2010).

67. M. Snyder, K. Drlica, DNA gyrase on the bacterial chromosome: DNA cleavage induced by oxolinic acid. *J. Mol. Biol.* **131**, 287–302 (1979).

68. M. Malik, X. Zhao, K. Drlica, Lethal fragmentation of bacterial chromosomes mediated by DNA gyrase and quinolones. *Mol. Microbiol.* **61**, 810–825 (2006).

69. J. M. Pennington, S. M. Rosenberg, Spontaneous DNA breakage in single living Escherichia coli cells. *Nat. Genet.* **39**, 797–802 (2007).

70. D. Edelmann, B. A. Berghoff, A shift in perspective: A role for the type I Toxin TisB as persistence-stabilizing factor. *Front. Microbiol.* **13**, 871699 (2022).

71. J. A. Booth, M. Špírek, T. A. Lobie, K. Skarstad, L. Krejci, M. Bjørås, Antibiotic-induced DNA damage results in a controlled loss of pH homeostasis and genome instability. *Sci. Rep.* **10**, 19422 (2020).

72. E. Z. Reyes-Fernández, S. Schuldiner, Acidification of cytoplasm in Escherichia coli provides a strategy to cope with stress and facilitates development of antibiotic resistance. *Sci. Rep.* **10**, 9954 (2020).

73. B. Van den Bergh, H. Schramke, J. E. Michiels, T. E. P. Kimkes, J. L. Radzikowski, J. Schimpf, S. R. Vedelaar, S. Burschel, L. Dewachter, N. Lončar, A. Schmidt, T. Meijer, M. Fauvart, T. Friedrich, J. Michiels, M. Heinemann, Mutations in respiratory complex I promote antibiotic persistence through alterations in intracellular acidity and protein synthesis. *Nat. Commun.* **13**, 546 (2022).

74. E. Padan, S. Schuldiner, [27] Intracellular pH regulation in bacterial cells. *Methods Enzymol.* **125**, 337–352 (1986).

75. A. M. Dri, P. L. Moreau, Control of the LexA regulon by pH: Evidence for a reversible inactivation of the LexA repressor during the growth cycle of Escherichia coli. *Mol. Microbiol.* **12**, 621–629 (1994).

76. F. J. R. Sousa, L. M. T. R. Lima, A. B. F. Pacheco, C. L. P. Oliveira, I. Torriani, D. F. Almeida, D. Foguel, J. L. Silva, R. Mohana-Borges, Tetramerization of the LexA repressor in solution: Implications for gene regulation of the E.coli SOS system at acidic pH. *J. Mol. Biol.* **359**, 1059–1074 (2006).

77. A. Ketcham, P. L. Freddolino, S. Tavazoie, Intracellular acidification is a hallmark of thymineless death in E. coli. *PLOS Genet.* **18**, e1010456 (2022).

78. R. Weel-Sneve, K. I. Kristiansen, I. Odsbu, B. Dalhus, J. Booth, T. Rognes, K. Skarstad, M. Bjørås, Single transmembrane peptide DinQ modulates membrane-dependent activities. *PLOS Genet.* **9**, e1003260 (2013).

79. J. P. Pribis, L. García-Villada, Y. Zhai, O. Lewin-Epstein, A. Z. Wang, J. Liu, J. Xia, Q. Mei, D. M. Fitzgerald, J. Bos, R. H. Austin, C. Herman, D. Bates, L. Hadany, P. J. Hastings, S. M. Rosenberg, Gamblers: An antibiotic-induced evolvable cell subpopulation differentiated by reactive-oxygen-induced general stress response. *Mol. Cell* **74**, 785–800.e7 (2019).

80. J. P. Pribis, Y. Zhai, P. J. Hastings, S. M. Rosenberg, Stress-induced mutagenesis, gambler cells, and stealth targeting antibiotic-induced evolution. *MBio* **13**, e0107422 (2022).

81. F. R. Blattner, G. Plunkett, C. A. Bloch, N. T. Perna, V. Burland, M. Riley, J. Collado-Vides, J. D. Glasner, C. K. Rode, G. F. Mayhew, J. Gregor, N. W. Davis, H. A. Kirkpatrick, M. A.

Goeden, D. J. Rose, B. Mau, Y. Shao, The complete genome sequence of Escherichia coli K-12. *Science* **277**, 1453–1462 (1997).

82. K. A. Datsenko, B. L. Wanner, One-step inactivation of chromosomal genes in Escherichia coli K-12 using PCR products. *Proc. Natl. Acad. Sci. U.S.A.* **97**, 6640–6645 (2000).

83. J. H. Davis, A. J. Rubin, R. T. Sauer, Design, construction and characterization of a set of insulated bacterial promoters. *Nucleic Acids Res.* **39**, 1131–1141 (2011).

84. F. Goormaghtigh, L. Van Melderen, Optimized method for measuring persistence in escherichia coli with improved reproducibility. *Methods Mol. Biol.* **1333**, 43–52 (2016).

85. I. Wiegand, K. Hilpert, R. E. W. Hancock, Agar and broth dilution methods to determine the minimal inhibitory concentration (MIC) of antimicrobial substances. *Nat. Protoc.* **3**, 163–175 (2008).

86. T. Oms, T. Schlechtweg, J. Cayron, L. Van Melderen, Population and single-cell analysis of antibiotic persistence in Escherichia coli. *J. Vis. Exp.* 10.3791/64550 (2023).

87. J. Schindelin, I. Arganda-Carreras, E. Frise, V. Kaynig, M. Longair, T. Pietzsch, S. Preibisch, C. Rueden, S. Saalfeld, B. Schmid, J.-Y. Tinevez, D. J. White, V. Hartenstein, K. Eliceiri, P. Tomancak, A. Cardona, Fiji: An open-source platform for biological-image analysis. *Nat. Methods* **9**, 676–682 (2012).

88. A. Ducret, E. M. Quardokus, Y. V. Brun, MicrobeJ, a tool for high throughput bacterial cell detection and quantitative analysis. *Nat. Microbiol.* **1**, 16077 (2016).

89. J. Cayron, A. Dedieu-Berne, C. Lesterlin, Bacterial filaments recover by successive and accelerated asymmetric divisions that allow rapid post-stress cell proliferation. *Mol. Microbiol.* **119**, 237–251 (2023).

90. F. Goormaghtigh, N. Fraikin, M. Putrinš, T. Hallaert, V. Hauryliuk, A. Garcia-Pino, A. Sjödin, S. Kasvandik, K. Udekwu, T. Tenson, N. Kaldalu, L. Van Reassessing the role of type II toxin-antitoxin systems in formation of Escherichia coli type ii persister cells. *mBio* **9**, e00640-18 (2018).